MEMORIA FINAL

BECA DE VERANO 2022

INSTITUTO DE ASTROFÍSICA DE CANARIAS

TÍTULO DEL PROYECTO: Inferring dynamical distinct components in nearby galaxies using velocity gradients

IP DEL PROYECTO: Begoña García-Lorenzo & Natacha Zanon Dametto

AUTORA: Alba Casasbuenas Corral

A.1. RESUMEN

Abstract

La cinemática estelar y del gas ionizado traza la estructura dinámica de las galaxias y restringe los procesos que impulsan su evolución. García-Lorenzo et al. (2015) desarrolló un enfoque sencillo para la estimación de la ubicación del centro cinemático de las galaxias utilizando los mapas de velocidad del gas ionizado de una pequeña muestra de galaxias usando el cartografiado de galaxias CALIFA. En este trabajo, hemos adaptado este método al cartografiado de galaxias MaNGA, usando una muestra mucho mayor de galaxias en el Universo Local. Además, hemos completado el análisis mediante el uso de mapas de velocidad tanto de las estrellas como del gas ionizado. Se han encontrado varios factores que causan desviaciones del movimiento de rotación pura en una galaxia, que a su vez se manifiestan como un desplazamiento entre su centro cinemático y su núcleo óptico. Dos de estos factores son las fusiones e interacciones de galaxias y su masa estelar.

A.2. SUMMARY

Abstract

The stellar and ionized gas kinematics trace the dynamical structure of galaxies and constrain the processes driving their evolution. García-Lorenzo et al. (2015) developed a simple approach for estimating the kinematic center location of galaxies using the velocity maps of the ionized gas of a small sample of galaxies using the CALIFA galaxy survey. In this work, we have adapted this method to the MaNGA galaxy survey, using a much larger sample of galaxies in the Local Universe. Moreover, we have completed the analysis by using both stellar and ionized gas velocity fields. We have found several factors that cause departures from pure rotational motions in a galaxy, manifesting as an offset between their kinematic center and optical nucleus. Two of these factors are galaxy mergers and interactions and stellar mass.

B. BACKGROUND AND CURRENT STATE OF THE TOPIC

Stellar and ionized gas kinematics are important tracers of the dynamical structure and overall evolution of galaxies. Some of the processes that lead to the formation and evolution of the galaxies are: interactions and mergers, the relative mass contribution of luminous and dark matter, the presence of supermassive black holes and their relationship with the large-scale properties of the host galaxies, the origin of kinematically decoupled components and of disk heating and the presence of pressure-supported ionized gas in bulges, the fraction of quiescent and/or disturbed galaxies or even the fraction of galaxies supported by rotation (see García-Lorenzo et al., 2015 for references).

Thanks to the advent of Integral Field Spectroscopy (IFS), it is now possible to obtain two-dimensional kinematics of the gas and stars of nearby galaxies and, with it, to better understand the processes that cause the different motions of the stars and gas present in these galaxies. The velocity maps obtained from IFS surveys allow us to identify regions where velocities change rapidly by computing the velocity gradient maps. For galaxies with regular kinematics dominated by rotation, these maps will present a single peak at the location of the kinematic center, which will coincide with the optical nucleus of the galaxy. On the other hand, the presence of extended structures or an offset between the kinematic center and the optical nucleus will indicate a departure from pure rotation.

García-Lorenzo et al. (2015) used CALIFA (the Calar Alto Legacy Integral Field Area Survey, Sánchez et al., 2012) to provide an overall characterization of the kinematic behaviour of the ionized gas of a small sample of galaxies (177 galaxies in total). They developed a method to calculate the velocity gradient maps and the kinematic center of the galaxies from the velocity maps. They found that an offset between the kinematic center and the optical nucleus was usually related to galactic mergers and that a structure in the gradient peak was usually related to the existence of a bar.

Ever since CALIFA, more surveys have used IFS techniques, reaching a more significant number of galaxies and obtaining velocity maps with better spatial and spectral resolution. Therefore, it would be interesting to repeat the analysis carried out in García-Lorenzo et al. (2015) with other galaxy surveys. Because this analysis has not been carried out yet with the MaNGA (Mapping Nearby Galaxies at Apache Point Observatory) Integral Field Spectroscopy (IFS) survey, which we will talk about in more detail in section D, we will use this survey to complete the research made in the reference paper, this time using a more significant sample and a higher spatial and spectral resolution, which will also allow us to study not just the ionized gas kinematics, but also the stellar component.

C. HYPOTHESIS AND OBJECTIVES

The aim of this work is to characterize the kinematic behaviour of the stellar component and ionized gas of the galaxies included in the MaNGA survey, using a similar methodology as the one implemented with galaxies from the CALIFA in García-Lorenzo et al. (2015).

For an ideal purely rotating disk galaxy, the rotation velocity varies with radius from the kinematic center, which is located in the galactic center, and it is settled by the radial distribution of mass within the galaxy. The kinematic center in rotating disk galaxies has, therefore, a zero rotation velocity and is the location of the largest velocity gradient in the galaxy. Using this reasoning we can calculate the kinematic center of a sample of galaxies, and according to its location in relation with the optical nucleus, we can identify the galaxies that diverge from pure rotation and try to find their causes.

Furthermore, García-Lorenzo et al. (2015) also found that galaxies with regular rotation have a single peak as the largest velocity gradient point. However, for galaxies with complex kinematics, the gradient image usually has more than one single velocity peak, and there are gradient structures that can also be related with a divergence from pure rotation, like bars, mergers, or AGN (Active Galactic Nucleus) hosts.

García-Lorenzo et al. (2015) only studied the ionized gas kinematics using the Hα emission line. However, there might also be significant differences between the motion of the gas and stellar content of the galaxies, so in this work we will study Hα, [OIII], and the stellar component, and see the differences between the ionized gas and the stellar kinematics in these galaxies.

Objectives

- To derive and analyse the velocity gradient distributions of a sample of galaxies included in the MaNGA survey, using the stellar and ionized gas velocity fields, focusing on both the Hα and [OIII] emission lines.
- To calculate the kinematic center location of each galaxy and compare it with the location of its optical nucleus.
- To label the galaxies according to their morphology, interaction status, and whether or not they are a confirmed AGN host according to the information available in the MaNGA Value-Added catalogs.
- To classify the galaxies according to their velocity gradient structures. This is fairly straightforward to classify by eye, but in order to work with large data samples, it is necessary to think of a way to automatize this.
- To identify and analyze the relationships between the kinematic center and optical nucleus distance, the velocity gradient structures, and the relevant properties of the galaxies in the sample.

Therefore, the structure of this work will be distributed as follows. In section D, we will describe the data sample used, taken from the MaNGA survey, as well as the value-added catalogs from which we obtain fundamental parameters for the galaxies (e.g. redshift, morphological type, interaction state, mass, etc.), and we will also detail the methodology used for the analysis, particularly how the gradient maps are obtained from the velocity maps from each galaxy. In section E, we will present the results of the distribution of the kinematic center of the galaxies studied, relating it to different galactic parameters for the full MaNGA sample and two sub-samples of galaxies. In section F, we will discuss the future work that could be conducted to complete the research done in this work. Finally, in section G, we will explain some conclusions.

D. MATERIAL AND METHODS

Data Sample: The MaNGA Survey

In this work, we use the MaNGA (Mapping Nearby Galaxies at Apache Point Observatory) IFS survey (Bundy et al., 2014). The MaNGA survey, which is one of the core programs in the fourth-generation Sloan Digital Sky Survey (SDSS-IV), uses the 2.5m Sloan Telescope in its spectroscopic mode, with 17 fiber-bundle integral field units (IFUs) that vary in diameter from 12" (19 fibers) to 32" (127 fibers). The survey began in 2014, aiming to investigate the internal kinematic structure and composition of gas and stars in a sample of 10,000 nearby galaxies with $M_* > 10^9 M_\odot$ and $\langle z \rangle < 0.15$. This survey will allow us to do a more statistical comprehensive analysis than the one performed with CALIFA in García-Lorenzo et al. (2015), which had a sample of 600 galaxies in total, and only reached a redshift range of $\langle z \rangle < 0.03$.

The MaNGA data-analysis pipeline (MaNGA DAP, Westfall et al., 2019) is the survey-led software package that has analysed all galaxy data produced by the MaNGA data-reduction pipeline (MaNGA DRP), in order to produce high-level, science-ready data products derived from MaNGA spectra. In this work, we use the maps of stellar, Hα, and [OIII] ionized gas kinematics produced by the MaNGA DAP of the full MaNGA sample of galaxies.

In order to classify the properties of the galaxies, we use data from the SDSS Value-Added catalogs. Firstly, for the basic parameters of each galaxy like the coordinates and the redshift, we use the **NSA-Sloan Atlas** (Blanton et al., 2011), a catalog of images and parameters of local galaxies derived from SDSS imaging. The MaNGA survey uses this catalog for targeting, and therefore all the galaxies observed have the parameters included in this catalog. For the information on the mass of each galaxy, we use the **MaNGA Pipe3D value-added catalog** (Sánchez et al., 2016). This catalog of spatially resolved and integrated properties of galaxies for MaNGA DR17 uses an IFU-focused analysis pipeline that provides information about the galaxies extracted from the MaNGA datacubes in an automatic way focusing on the stellar populations and the ionized properties.

For the morphological classification of the galaxies, we use the **MaNGA Morphology Deep Learning DR17 catalog** (Domínguez Sánchez et al., 2022). This morphological catalog of MaNGA galaxies obtained with Deep learning models allows us to classify the galaxies based on their T-Type, the probability of being a late-type galaxy P_LTG, the probability of being a lenticular galaxy P_ S0 and a visual classification VC. We divide the galaxies into S2 (late-type galaxies with strong spiral arms), S1 (late-type galaxies with weaker spiral arms), S0 (lenticular galaxies), E (elliptical galaxies) and Irr (galaxies that the AI couldn'could not classify correctly), following the recommendations included in the paper:

- S2: T-Type $>$ 3 AND P_LTG $\geq$ 0.5 AND VC=3
- S1: T-Type $>$ 0 AND T-Type $<$ 3 AND P_LTG $\geq$ 0.5 AND VC=3
- S0: T-Type $\leq$ 0 AND P_S0 $>$ 0.5 AND P_LTG $<$ 0.5 AND VC=2

- E: T-Type ≤ 0 AND P_S0 ≤ 0.5 AND P_LTG < 0.5 AND VC=1

In addition, we also record the parameters P_edge-on and P_bar; the former describes the probability of each galaxy being edge-on and the latter characterises the probability of them having a bar. To classify the galaxies according to their barred status, we divide them as Bar A for galaxies with a high probability of having a bar (P_bar>2/3), Bar B for those with a low probability of having a bar (P_bar<1/3) and Bar AB for those with an intermediate probability of having a bar.

Thirdly, in order to characterise the interacting or isolated nature of each of the galaxies, we use the **GEMA-VAC: Galaxy Environment for MaNGA Value-Added catalog**. (Argudo-Fernández et al., 2015). We define isolated galaxies (hereafter SIG: SDSS-based Isolated Galaxies) as galaxies that are assumed to have escaped serious influences from their nearest neighbours during a crossing time $t_{cc} \simeq 3\ Gyr$ (Verdes-Montenegro et al., 2005). This is marked in the catalog as the galaxies that have no neighbours found in the characterization of the Large-Scale Structure (LSS) environment by all neighbours within 500 km/s line-of-sight velocity difference up to 1 Mpc projected distance.

The isolation degree as defined in this study is more conservative than the one used in García-Lorenzo et al. (2015), where they visually identified signatures of interactions like tidal tails and nearby companions with spatially projected separation ≤ 100 kpc and systemic velocity difference ≤ 1000 km s^{-1}, in order to identify ongoing one-to-one galaxy interactions, mergers showing tidal features and compact groups of galaxies. This difference will make the comparison with García-Lorenzo et al. (2015) harder. However, the study of isolated galaxies as defined in this study will also provide a new branch of study and new opportunities for future work that will be discussed later.

Finally, we use the **MaNGA AGN catalog** (Comerford et al., 2020) to identify the confirmed AGN hosts in the MaNGA sample. This catalog was constructed from the first six thousand galaxies observed with MaNGA, through mid-2018, and presents the robust identification of 406 AGNs using four different approaches: Wide-field Infrared Survey Explorer (WISE) mid-infrared colour cuts, Swift/BAT hard X-ray sources, NVSS/FIRST 1.4 GHz radio sources, and SDSS broad emission lines.

Methodology

For the analysis of the MaNGA data used in this work, we have used the Marvin Tools python package (Cherinka et al., 2019). This allows us to access the MaNGA DAP maps of every studied galaxy included in the MaNGA DAPall catalog. In this work, we focus on the velocity maps of the stellar component and the ionized gas. For the latter, we study the velocity maps of the emission lines Hα (6564 Å), an important tracer of star formation, as well as [OIII] (5008 Å), an important emission line in AGN studies (Kauffmann et al., 2003). For the stellar continuum, we analyse the stellar velocity field.

Using these velocity maps, we mask the pixels flagged by the MaNGA DAP as DONOTUSE, that is, the spaxels which are not recommended to use for science. This flag includes the

spaxels where there is no coverage or low coverage, the major contributing fiber is dead, there is a foreground star, there is no fitted value, there was a mathematical error in computing the value, the attempted fit failed, or the fitted value was too near an imposed boundary. Furthermore, in order to only use spaxels where there is a good measurement, we impose that the mean g-band weighted signal-to-noise ratio per pixel is more than 6 in each of the spaxels of the map, masking the ones that do not fit this criterion. Finally, to deal with the outlier velocity values that were not masked with the previous criteria and would saturate the gradient image, we mask the spaxels where the absolute value of the velocity falls outside the interquartile range of the map values, identifying them as outliers. Once the map has been altered, we discard the maps that have been left with a number of pixels that is too low to make a good analysis. This limit has been determined as 160 pixels at least in all three studied velocity maps after the visual inspection of an arbitrarily high number of velocity and gradient maps.

The next step was to identify the optical nucleus of the galaxy as the point where the stellar continuum of the galaxy has a higher value. This point should coincide with the center of the image because of the configuration of Manga. We add a flag to identify the galaxies where this does not happen in order to inspect them further later, and we do not include these in our analysis.

Afterwards, we can calculate the velocity gradient map of each of the studied components as the average derivative of the velocity fields. This is computed by calculating the average absolute difference of the obtained velocity for each spectrum with the velocity of the surrounding regions. This was done by adapting the IDL code used in García-Lorenzo et al. (2015) into Python for the MaNGA data. The resulting velocity gradient image accentuates the regions of the galaxy where the velocity changes rapidly. Therefore, for galaxies showing regular motions, the peak of the velocity gradient image should indicate the location of the Kinematic center. This procedure works for regular velocity fields. However, for complex kinematics, there is usually more than a single velocity gradient peak, indicating that there are several regions where radial velocities are changing rapidly. When the velocity gradient distribution shows the optical nucleus surrounded by a ring-like or bar-like structure of large velocity gradient values. This is identified, therefore, as a sign of departure from pure rotation.

For the estimation of the Kinematic Center, we follow the same procedure as García-Lorenzo et al. (2015). We choose a square region of fixed size around the optical nucleus (which for galaxies with pure rotation should coincide with the largest velocity peak) and then we select the pixels with a velocity gradient value larger than 1σ over the average velocity gradient inside this box. The KC is estimated from the weighted average location of the selected positions defining the peaks or structures of the velocity gradient map, using as weights the velocity gradient value at each location. The uncertainty in the location of the KC is estimated assuming different radii when choosing the box, from half the PSF size to double the PSF size, and calculating the standard deviation of all the KC locations obtained with each of them.

Velocity and Gradient Map Examples

In this section we will include some examples of velocity and gradient maps of a small number of galaxies, in order to get an idea of how the maps look and to better understand how to proceed with the analysis, particularly to think of ways to identify the velocity gradient structures in the different gradient maps. We also include an image of the optical SDSS image of each of the galaxies, with the hexagon representing the area of the galaxy covered in the MaNGA survey.

Firstly, in figure 1, we include an example of a clear disk galaxy with a clear rotation. Even though this is a barred galaxy, it behaves like a rotating disk and doesn't seem to have a strong structure in the gradient peak.

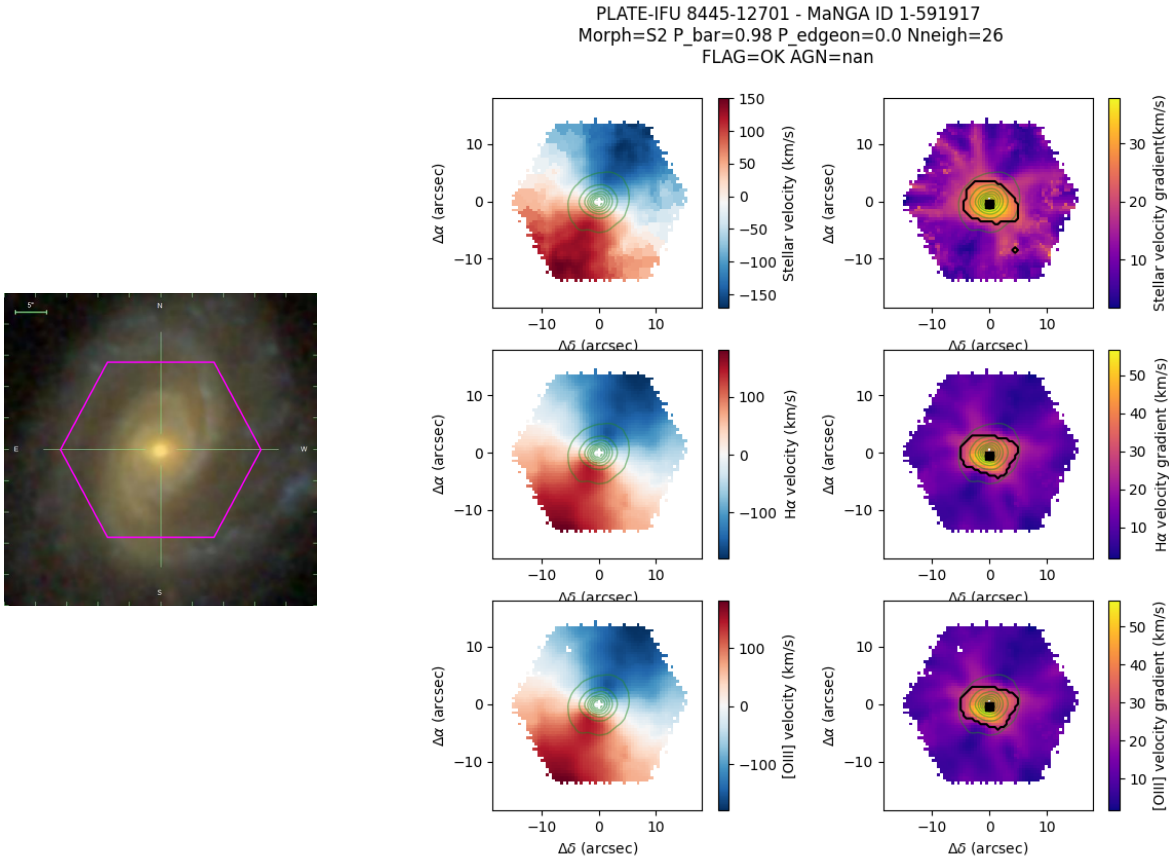

Fig. 1 – Left: SDSS three-color image of the MaNGA galaxy 8445-12701. Right: in the first column, the velocity maps of each of the components studied in the galaxy, and in the second column, the gradient map. From top to bottom, the maps are made using the stellar, Hα and [OIII] components, respectively. The area inside the thick black contour holds the velocity gradient pixels used to estimate the KC location through the average of their positions weighted by their gradient values. Contours from the stellar continuum are overlapped in green. The white cross marks the position of the optical nucleus and the black circle indicates the estimated position of the kinematic center.

However, it is not always the case that there is a strong single peak in the gradient map that marks the kinematic center. Sometimes this peak has a structure like a bar or a ring. In García-Lorenzo et al. (2015) they found that these structures could be related with the presence of kinematic instabilities like a bar. We will now analyze a few examples of how these structures might manifest in the different gradient maps, by presenting some gradient maps of strongly barred galaxies, created following the same methodology and using the same design as in figure 1.

In figure 2, for example, we represent a galaxy where the kinematic asymmetries caused by the bar manifest as a clear structure in the gradient map peak. We can appreciate, particularly in the maps made with the ionized gas components, that there seem to be two gradient peaks, in long structures perpendicular to the bar. Despite the clear deviation from pure rotation in the gradient map, the kinematic center is still estimated near the optical nucleus. This is a good example of why the information about the structures in the gradient maps peaks is necessary to complement the information about the kinematic center location.

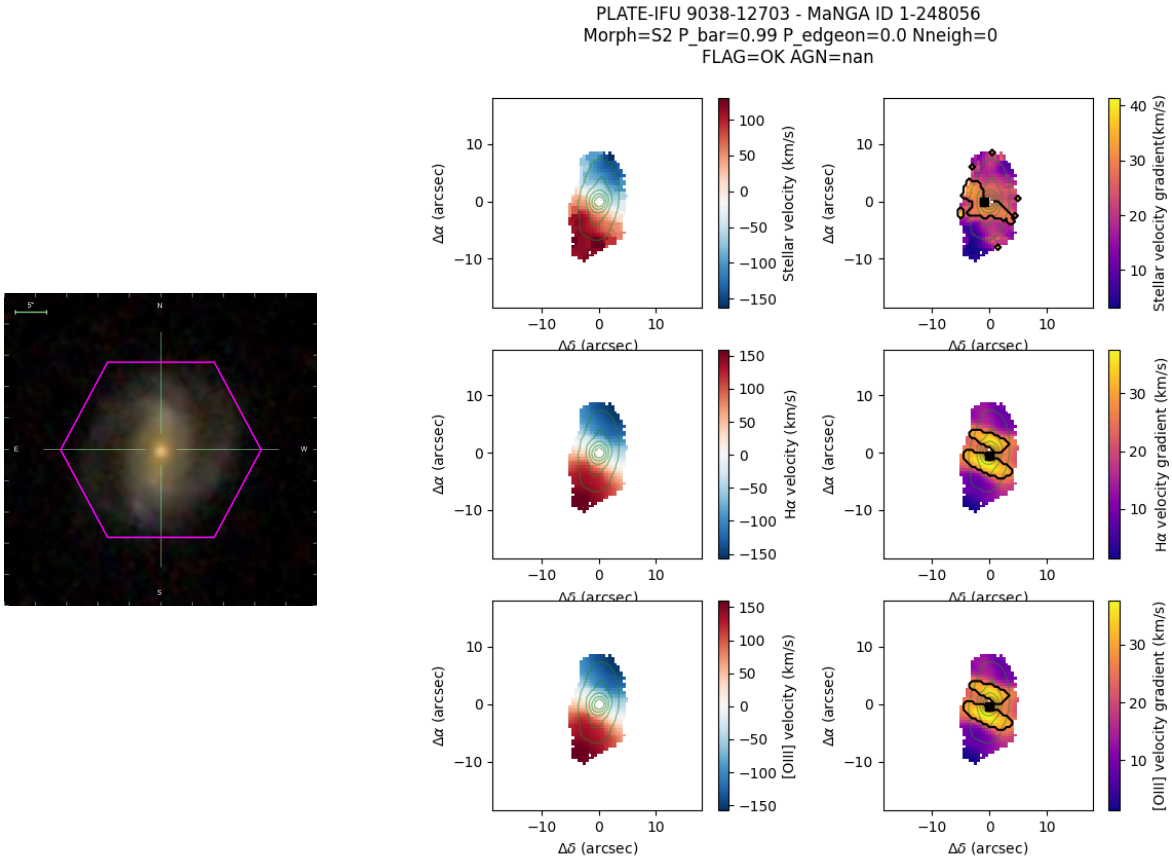

Fig. 2 – Left: SDSS three-color image of the MaNGA galaxy 9038-12703. Right: velocity and gradient maps of each of the components studied in the galaxy. From top to bottom, the maps are made using the stellar, Hα and [OIII] components, respectively. The design follows the description of figure 1.

In figure 3 we represent another strongly barred galaxy, where the structure in the gradient maps, particularly of the ionized gas component, has a ring-like structure. This does not manifest as clearly in the stellar velocity component, which is a clear example of how many times the stars and the ionized gas have different motions, and it is important to study the different components separately.

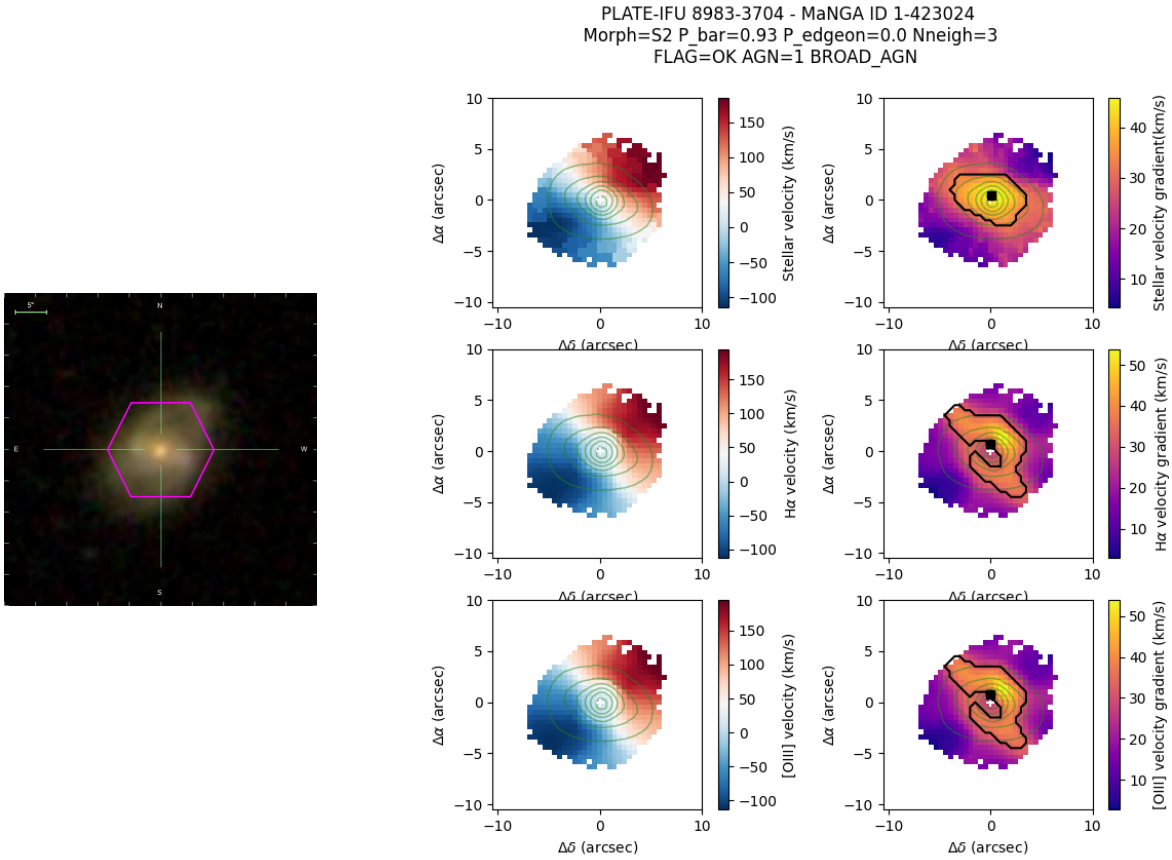

Fig. 3 – Left: SDSS three-color image of the MaNGA galaxy 8983-3704. Right: velocity and gradient maps of each of the components studied in the galaxy. From top to bottom, the maps are made using the stellar, Hα and [OIII] components, respectively. The design follows the description of figure 1.

In figure 4, we can see that the MaNGA survey focused on the center of the galaxy, where the bar took up most of the space. This manifests in the gradient peak structure as a long bar in the direction of the bar. Once again, we can appreciate this structure more clearly when studying the ionized gas component. Moreover, it is interesting to appreciate that the structure in the stellar component is slightly tilted with respect to the ionized gas component, showing once again this difference between the stellar and ionized gas motion inside the galaxy.

The previous figures are just a small number of examples from our full sample. While it would be interesting to inspect them one by one, this option is not viable with our sample,

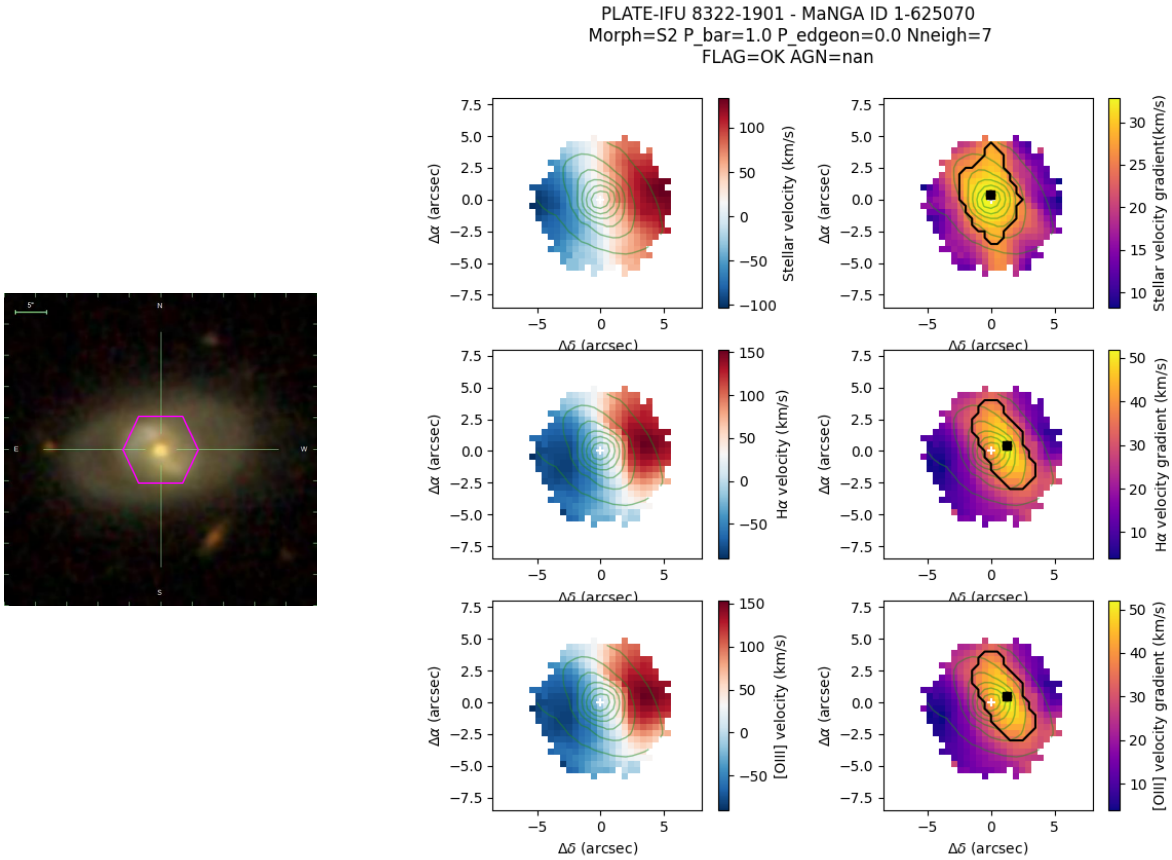

Fig. 4 – Left: SDSS three-color image of the MaNGA galaxy 8322-1901. Right: velocity and gradient maps of each of the components studied in the galaxy. From top to bottom, the maps are made using the stellar, Hα and [OIII] components, respectively. The design follows the description of figure 1.

which has more than ten thousand galaxies. Therefore, it is important to think of a way to automatise the classification of the gradient structures of each galaxy, in order to have it as a complementary value to the kinematic center position.

During the course of this work, we have tried different approaches to the identification and classification of the gradient peak structures. Most of these approaches have been based in trying to find the correlation between the location of the pixels used to estimate the KC location and their gradient values, and a hypothetical perfect single gradient peak distribution. However, the tried approaches have failed, and we have identified a number of challenges that make this process particularly difficult:

- We have been unable to find a single galaxy with a perfect single peak distribution, and even the ones that seemed like it after a visual inspection didn't work as a reference. This makes sense, because galaxies are not just rotating disks, but rather a combination of several structures. However, this makes it harder to find a way to automatize the process.
- The gradient peak structures, while easy to identify after a quick visual inspection, are

very varied, and this diversity makes it very difficult to adapt a criteria that works to identify all the deviations from a clear single gradient peak.

- Even after the quality cuts applied in this work, some of the velocity maps have border problems, saturated pixels and a large masked regions in the center of the velocity maps that make the gradient map have even stranger gradient peak structures, probably because they are not being calculated correctly.

These challenges can be addressed in the future by finding the algorithm that allows to correctly identify the shape of the velocity gradient peaks, and fine-tuning the maps in order to minimize the errors and better define the gradient peak structures in all of the galaxies in the sample.

E. RESULTS AND DISCUSSION

Full Data Sample

First of all, we focus on the results obtained with the full MaNGA sample. There are 10734 galaxies in the full MaNGA sample, of which 2535 galaxies are discarded from the analysis: 671 are flagged with having the optical nucleus far from the center of the image, and 1864 have velocity maps too small to analyse correctly. Therefore we are left with a total sample size of 8589 galaxies.

In figure 5 we represent a histogram with the morphological distribution of all the galaxies, as well as the mass distribution of the galaxies that we study and their redshift distribution. We also divide the galaxies according to their interacting status as SIG or interacting galaxies, and according to their bar probability.

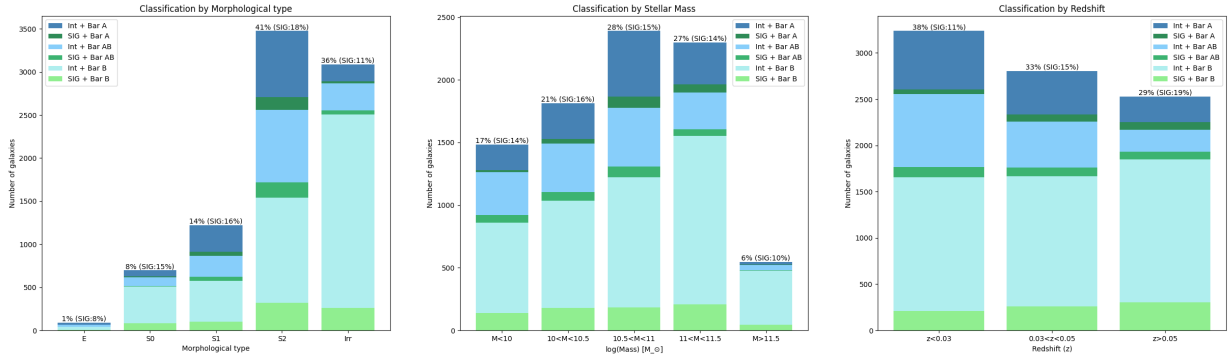

Fig. 5 – Distribution of the full MaNGA sample of galaxies according to their morphological classification, their stellar mass and their redshift. In the histograms we mark the number of galaxies in each classification according to their barred and interacting status, with blue representing interacting galaxies and green, the SIG galaxies, and the darker to lighter tones, stronger to weaker bar probabilities. Above each bar is the percentage of galaxies from the full sample that belongs to each category, and in parentheses is the percentage of the galaxies in the category that are classified as SIG.

Using this sample of all the MaNGA galaxies, we calculate the optical nucleus and kinematic center for each galaxy, using the methodology described in the previous section. Like we explained earlier, the kinematic center should coincide with the optical nucleus for a purely rotating galactic disk.

We present in figure 6 the offset between the optical nucleus and the kinematic center, which can indicate a departure from pure rotation, calculated with each of the components studied: the stellar kinematics and the ionized gas, both for Hα and [OIII]. We also present the offset between the kinematic center calculated from each component, which can identify processes that make the different components have different kinematics. We use the fiber size of the MANGA survey (2") as the minimum distance to report a possible offset, and double this size (4") as the minimum distance to report an offset.

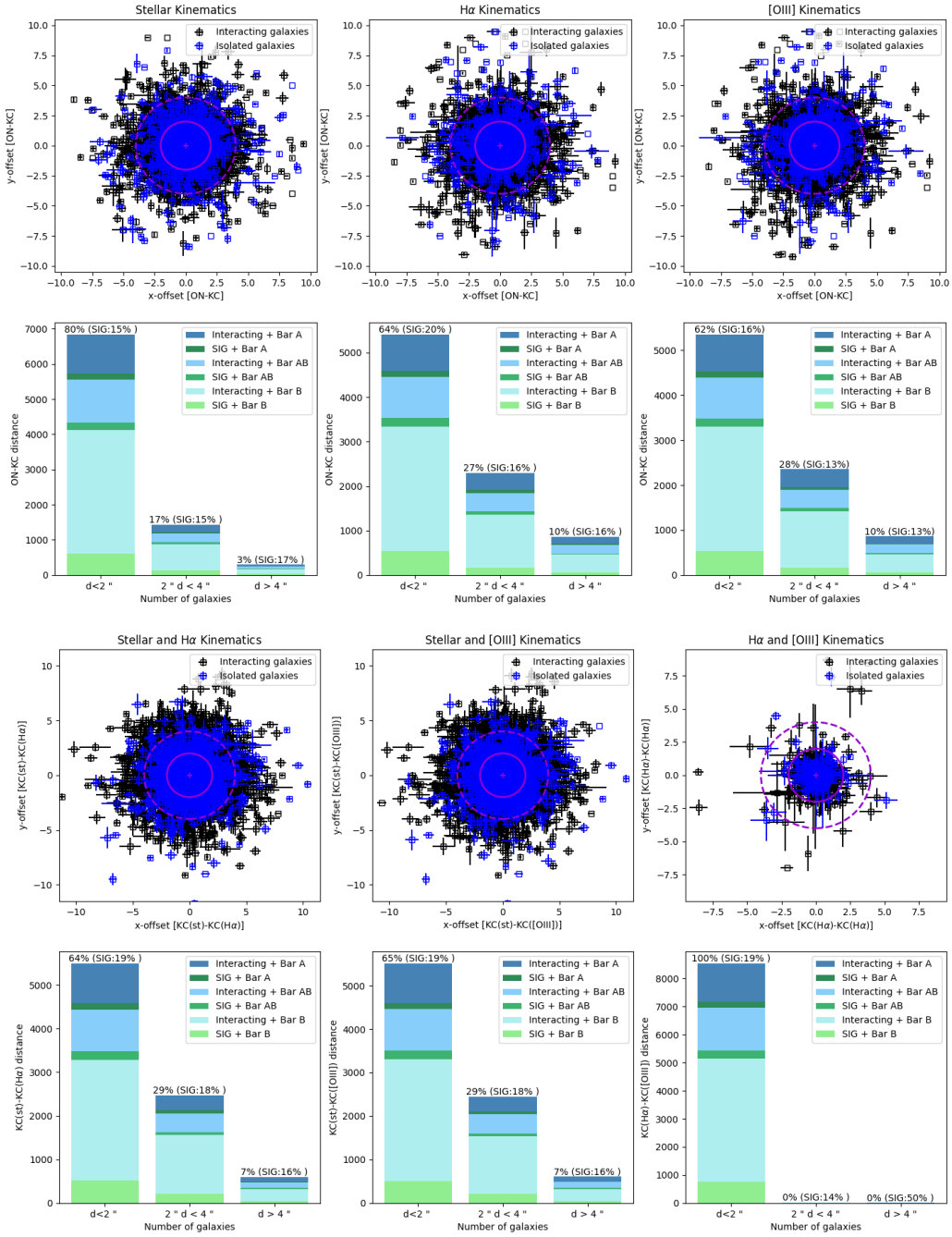

Fig. 6 – Top: Offset between the Optical Nucleus and the Kinematic Center of the full MaNGA sample of galaxies, calculated from the kinematics of the different components: the stellar continuum, Hα and [OIII]. Bottom: Offset between the Kinematic Centers calculated with each of the components studied. The purple lines represent the 2" mark and the 4" mark to report significant offsets. In the histograms beneath each offset graph we mark the number of galaxies in each offset range, with blue representing interacting galaxies and green, the SIG galaxies, and the darker to lighter tones, stronger to weaker bar probabilities. Above each bar is the percentage of galaxies from the full sample that belongs to each category, and in parentheses is the percentage of the galaxies in the category that are classified as SIG.

it is important to note that there are many differences that make it hard to compare figure 6 with the results published in García-Lorenzo et al. (2015). First of all, in the reference paper the analysis was just made using Hα kinematics, while we've used three different components, which makes this a more complete analysis of the kinematics. Moreover, it is important to bear in mind that in this work we are defining the isolated galaxies (SIG) applying stricter criteria, while in García-Lorenzo et al. (2015) they identified the more obvious mergers. Finally, it is important to note that the MaNGA survey is a deeper survey than the CALIFA survey, so we'd be comparing galaxies from a different range of redshifts.

Despite the differences between the analysis, it is possible to detect certain notable aspects in figure 6. While in García-Lorenzo et al. (2015) they identified a direct relationship between galaxies with significant offsets between the optical nucleus and their kinematic center and their interacting status, it is interesting to note that in our analysis the percentage of isolated galaxies (SIG) in each offset range stays mainly constant. It would be interesting to conduct some further research onto what is causing these offsets in the isolated galaxies. It would also be advantageous for our research to find a catalog with information on the interacting status of the galaxies in a more direct, visual way, not so strict, in order to better understand the effect of current mergers on the kinematic center - optical nucleus offset.

In order to better compare the results obtained in this work with the CALIFA results from the reference paper, we can focus on a sub-sample with low redshifts, choosing only the galaxies with redshifts lower than 0.03. This way, the galaxies studied in this work will be in the same redshift range as the ones studied in García-Lorenzo et al. (2015).

Low Redshift sub-sample

In the low redshift sample, defined as the galaxies with a redshift lower than 0.3, there is a total of 4197 galaxies, of which 1313 are discarded: 507 because of their optical nucleus location and 806 because of the velocity map size. This leaves us with a sub-sample size of 3250 galaxies, an improvement from the 177 galaxies that were studied in García-Lorenzo et al. (2015).

We present in figure 7 the offset between the optical nucleus and the kinematic center for each of the components studied, as well as the offset between the kinematic center calculated from each component, limiting the analysis to the low redshift sub-sample, following the same analysis used for figure 6. Once again, the significant offsets, identified as those higher than double the fiber size of the MaNGA survey (4"), are a sign of a departure from pure rotation for each component of the galaxy.

While we still have the problem of the difference of the definition of interacting galaxies in both works, the results presented in figure 7 are better for the comparison with the results obtained in the reference paper, presented in figure 8.

We can identify the same tendencies in figure 7 as the ones we identified in the results using the full MaNGA sample. it is not so clear in this work that it is possible to make a direct correlation between the interacting status of the galaxies and the offsets between their kine-

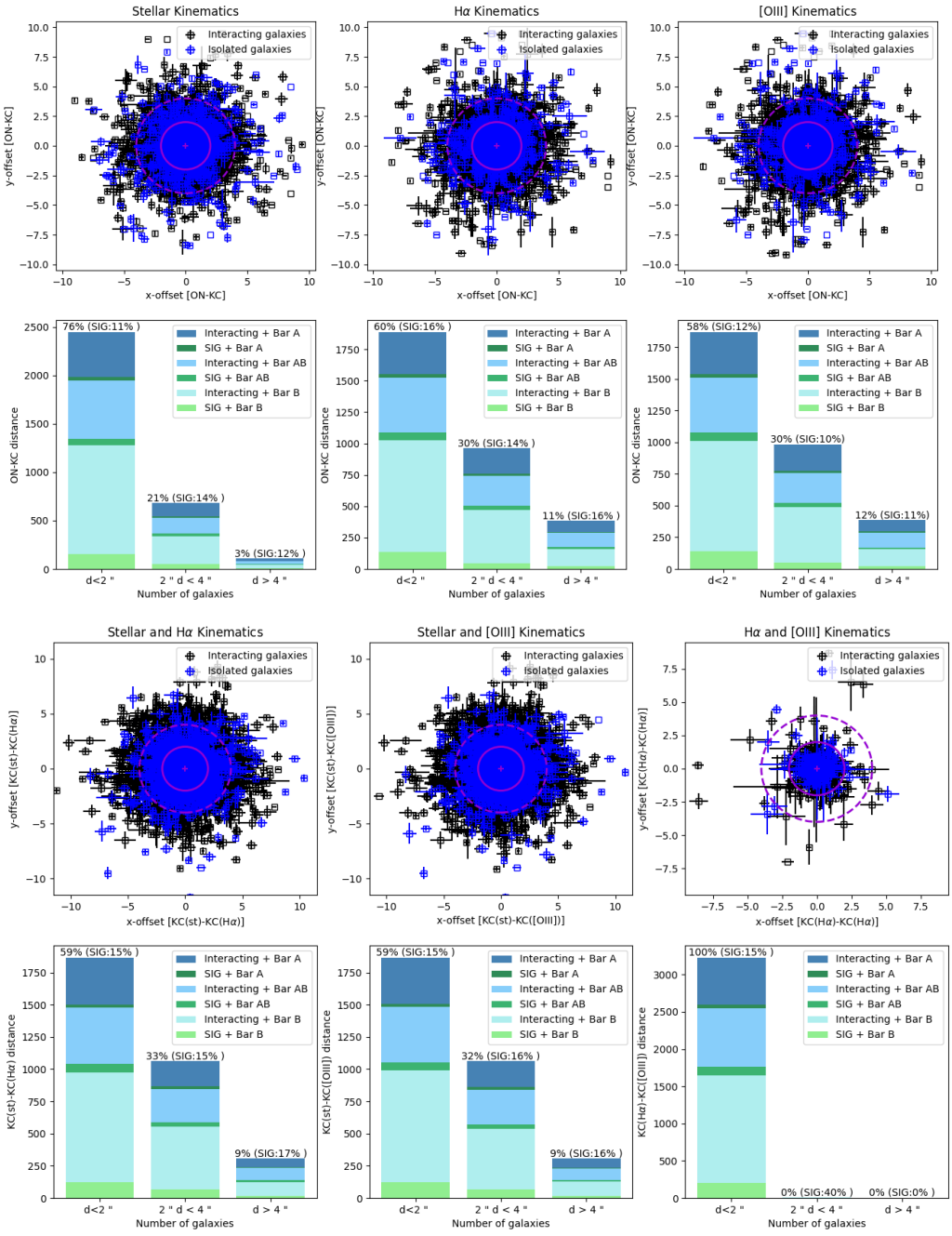

Fig. 7 – Top: Offset between the Optical Nucleus and the Kinematic Center of the low redshift MaNGA sample of galaxies, calculated from the kinematics of the different components: the stellar continuum, Hα and [OIII]. Bottom: Offset between the Kinematic Centers calculated with each of the components studied. The purple lines represent the 2" mark and the 4" mark to report significant offsets. In the histograms beneath each offset graph we mark the number of galaxies in each offset range, with blue representing interacting galaxies and green, the SIG galaxies, and the darker to lighter tones, stronger to weaker bar probabilities. Above each bar is the percentage of galaxies from the full sample that belongs to each category, and in parentheses is the percentage of the galaxies in the category that are classified as SIG.

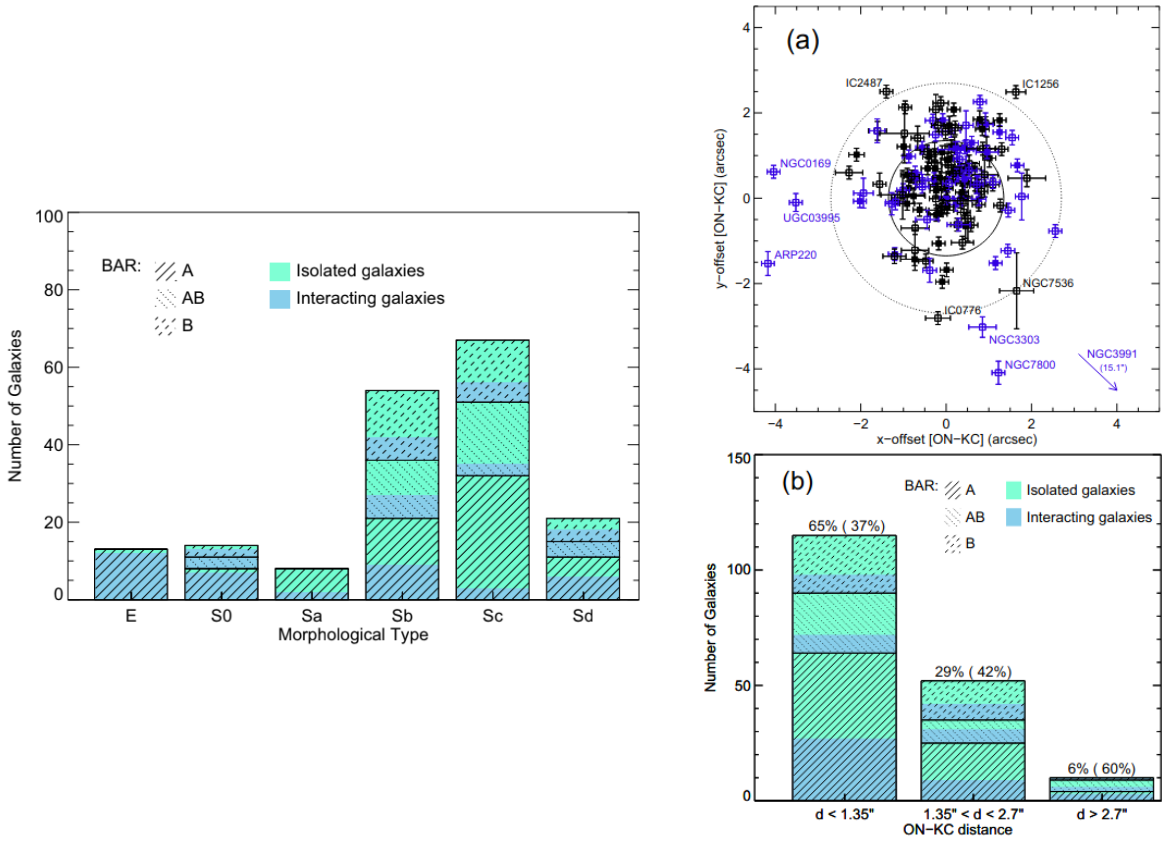

Fig. 8 – Morphology distribution (left) and and offset between the optical nucleus and the Hα kinematic center (right) obtained with the CALIFA data in García-Lorenzo et al. (2015), using a sample of 177 galaxies. The morphological classification of the galaxies is divided in ellipticals (E), lenticulars (S0) and spirals (Sa, Sb, Sc, Sd). The barred status is divided into A (strong bar), AB (weak bar) and B (no bar), and the interacting galaxies are identified as those with strong visible mergers.

matic centers and optical nuclei. Further research is needed to determine the cause behind these offsets.

Finally, because of the previous study's results relating offsets with direct interactions, it would be interesting to study the SIG galaxy sub-sample, to figure out the reason behind the offsets between the kinematic center and optical nucleus of isolated galaxies.

SDSS-Isolated Galaxies sub-sample

As we described earlier, SIG galaxies are defined as those where no neighbours are found in the characterization of their LSS environment in the GEMA-VAC catalog (Argudo-Fernández et al., 2015). In this section, we will not get this sub-sample from the full MaNGA sample, but rather just the first six thousand galxies observed with MaNGA, through mid-2018, in order to be able to also study their AGN status with the MaNGA AGN catalog (Comerford et al., 2020), as was described in section D. This will be interesting because interactions are one of the main triggers for AGNs (Ellison et al., 2011), so by studying isolated active

galaxies, we can start to raise the question of what triggered their nuclear activity.

In this sub-sample of the entire MaNGA sample there is a total of 1122 galaxies, of which 390 are discarded: 137 because of their optical nucleus location and 253 because of their velocity map size. This leaves us with a sub-sample size of 818 galaxies.

In figure 9, we represent a histogram with the morphological distribution of all the galaxies, as well as the mass distribution of the galaxies that we study and their redshift distribution. We also divide the galaxies according to their AGN status and according to their bar probability.

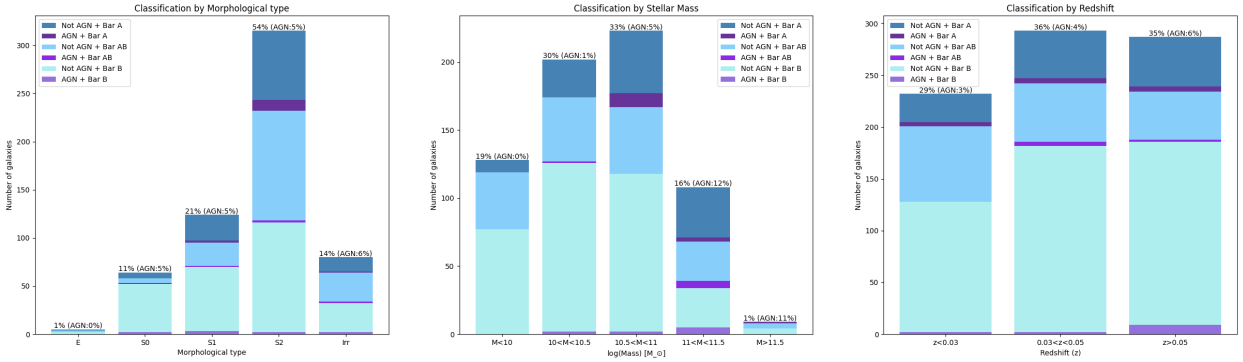

Fig. 9 – Distribution of the SIG MaNGA sample of galaxies according to their morphological classification, their stellar mass and their redshift. In the histograms we mark the number of galaxies in each classification according to their barred and AGN status, with blue representing non-AGN galaxies and purple, the AGNs, and the darker to lighter tones, stronger to weaker bar probabilities. Above each bar is the percentage of galaxies from the sample that belongs to each category, and in parentheses is the percentage of the galaxies in the category classified as AGN.

We can appreciate from figure 9 that there is not such a big number of AGNs in the SIG sub-sample (only 33 galaxies out of 406 total confirmed AGNs), but it will still be very interesting to study this isolated AGN sub-sample in order to discover what the cause behind their nuclear activity is.

Using this sample of isolated galaxies, we can proceed to calculate the optical nucleus and kinematic center of each galaxy like we've described before, remembering that an offset between these two points is a signal of a deviation from a purely rotating galactic disk.

We present in figure 10 the offset distribution between the optical nucleus and the kinematic center calculated with each of the components studied: the stellar kinematics and the ionized gas, both for Hα and [OIII], as well as the offset between the kinematic center calculated from each component, this time for the SIG sub-sample, using the same analysis than with the previous two samples.

In figure 10 we can appreciate that, as we expected from the previous figures, there is still a significant percentage of isolated galaxies with significant offsets. While it is true that the AGN proportion seems to be slightly higher for galaxies with bigger offsets, this is just a

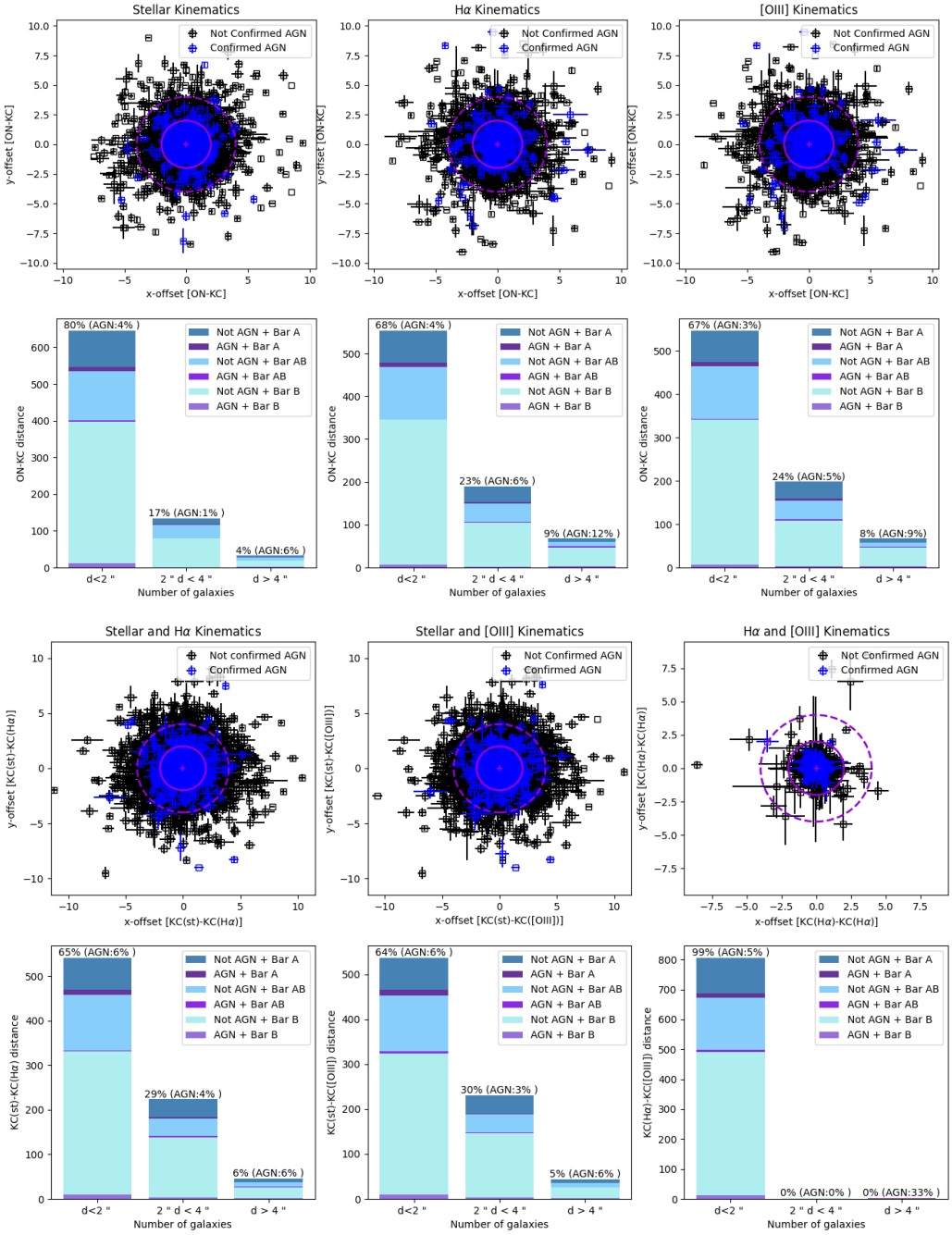

Fig. 10 – Top: Offset between the Optical Nucleus and the Kinematic Center of the SIG MaNGA sample of galaxies, calculated from the kinematics of the different components: the stellar continuum, Hα and [OIII]. Bottom: Offset between the Kinematic Centers calculated with each of the components studied. The purple lines represent the 2" mark and the 4" mark to report significant offsets. In the histograms beneath each offset graph we mark the number of galaxies in each offset range, with blue representing non-AGN galaxies and purple, the AGNs, and the darker to lighter tones, stronger to weaker bar probabilities. Above each bar is the percentage of galaxies from the full sample that belongs to each category, and in parentheses is the percentage of the galaxies in the category classified as AGN.

preliminary study and we cannot affirm that there is a correlation behind the offsets and the nuclear activity only with the results obtained with this plot; however it would also be an interesting subject for further research.

Finally, in order to shine more light into what the cause of the offsets in SIG galaxies might be, we can compare the morphological, mass and redshift distribution of the SIG galaxies that present no offsets (a total of 3004 galaxies) with the distribution of the SIG galaxies that present a significant offset in any of their components (a total of 534 galaxies). This way, we can easily identify if the morphology, mass or redshift of the galaxies might have any effect on the existence of an offset between the optical nucleus and the kinematic center, as well as between the kinematic centers of the different components. This is represented in figure 11.

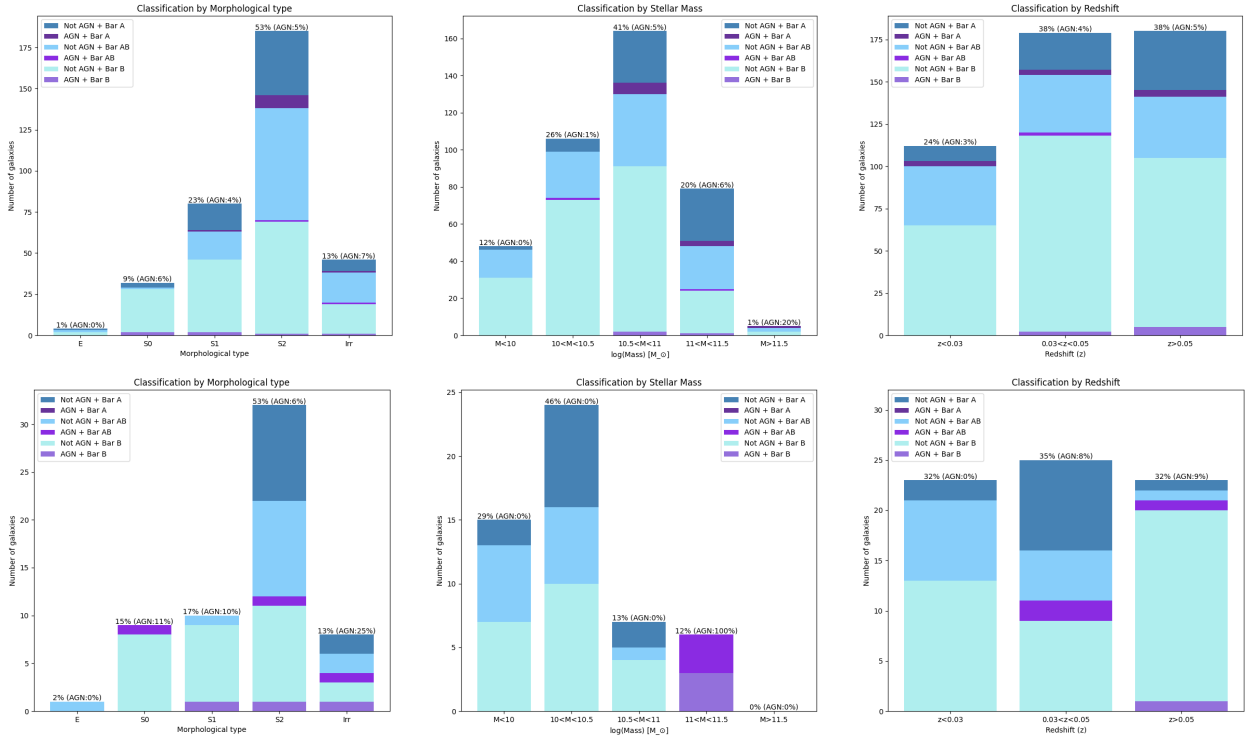

Fig. 11 – Comparison of the morphological, stellar mass and redshift distributions of the SIG MaNGA sample of galaxies according to their kinematic offsets. Top: Distribution of the SIG MaNGA sample of galaxies with an offset in any of the six components from figure 10 according to their morphological classification, their stellar mass and their redshift. Bottom: Distribution of the SIG MaNGA sample of galaxies with an offset in one or more of the six components from figure 10, according to their morphological classification, their stellar mass and their redshift. In the histograms we mark the number of galaxies in each classification according to their barred and AGN status, with blue representing non-AGN galaxies and purple, the AGNs, and the darker to lighter tones, stronger to weaker bar probabilities. Above each bar is the percentage of galaxies from the sample that belongs to each category, and in parentheses is the percentage of the galaxies in the category classified as AGN.

While this is just a quick preliminary look into the isolated galaxy distributions according to their kinematic offsets, in figure 11 it is easy to appreciate that the most obvious change

between the two samples is in the stellar mass distribution. The galaxies that present significant offsets are primarily low-mass galaxies, the entire mass distribution is shifted towards the lower masses. This makes sense with the theory, given that lower mass galaxies might not have reached the dynamical equilibrium needed for them to move as pure rotating galaxy disks.

Therefore, while there is still much work to be continued, we can affirm that there are other parameters which can cause kinematic offsets apart from the interacting status of the galaxy. One of these factors might be the stellar mass of the galaxies, and with it, other factors that contribute to the lack of dynamical equilibrium.

Moreover, we have checked that for certain high-mass galaxies, there is an error by classifying them as isolated with them being clear visual mergers. This strengthens the necessity to find a better definition of isolation and interaction for these galaxies, given that the current definitions used using the GEMA-VAC catalogue aren't appropriate for the needs of this work.

E. FUTURE WORK

For this work, we have generated a table for the full sample of galaxies and another one for the sub-sample of galaxies observed through mid-2018 used in the MaNGA AGN catalog, with all the relevant information for each of the galaxies in the samples, in order to make any future analysis easier. These tables record the information detailed in table 1. By reading these tables, it is easy to define the different sub-samples of galaxies used detailed throughout the work, and carry on any further kinematic analysis needed.

Next, we will list some ideas for further research using this work as a base.

- To perfect the kinematic analysis and reduce the border problems, saturated pixels and large masked regions in the velocity and gradient maps, and when that's not possible, to correctly identify the untrustworthy maps.
- To study the possibility of reviewing the largest possible number of maps in order to check their reliability and their structure.
- To think of an automatic way to identify the different gradient peak structures for the full sample of galaxies, in order to add this parameter to the analysis.
- To study in more detail the individual gradient maps of interesting sub-samples of galaxies, like for example the SIG that present significant offsets, or the SIGs that are also identified as AGNs.
- To do a parallel study of the same galaxies using data from other galaxy surveys like MUSE, which has a higher resolution than MaNGA and could therefore do a more thorough analysis of the same objects.
- To find a way to define more direct mergers in order to be able to do a better comparison with the reference paper and check if we find the same effect on the kinematic offsets that they found in García-Lorenzo et al. (2015).
- To do a deeper study on the SDSS-Isolated Galaxies.
- To relate the kinematic offsets found in these works with other relevant parameters apart from the barred and interacting status. As an idea, it could be interesting to relate this with the velocity map asymmetries found and detailed in Feng et al. (2022).

Name	Description
PLATEIFU	Plate+ifudesign name for this object
MANGAID	MaNGA ID for this object
OBJRA	Right ascension of the science object in J2000
OBJDEC	Declination of the science object in J2000
NSA_Z	Heliocentric redshift
NSA_ZDIST	Distance estimate, mulitply by c/Ho for Mpc
MORPH	Morphological classification of the object
P_BAR	Probability of having a bar signature, trained with GZ2 catalog.
P_EDGEON	Probability of being edge-on, trained with the GZ2 catalog.
P_MERGE	Probability of mergers classified by the Galaxy Zoo project
NNEIGH	Number of LSS associations
Q_NN	Tidal strength of the 1st nearest neighbour
Q_LSS	Tidal strength of the LSS
LOGMASS	Integrated stellar mass in units of the solar mass in log scale
AGN	Number of catalogs in which the object is detected as an AGN.
AGN_CLASS	catalogs in which the object is detected as AGN
KCRA_ST	Distance (") in RA between the KC with the stellar component and the ON
KCDEC_ST	Distance (") in DEC between the KC with the stellar component and the ON
KCRA_ST_ERR	KCRA_ST uncertainty
KCDEC_ST_ERR	KCDEC_ST uncertainty
KCRA_HA	Distance (") in RA between the KC with the Hα component and the ON
KCDEC_HA	Distance (") in DEC between the KC with the Hα component and the ON
KCRA_HA_ERR	KCRA_HA uncertainty
KCDEC_HA_ERR	KCDEC_HA uncertainty
KCRA_OIII	Distance (") in RA between the KC with the [OIII] component and the ON
KCDEC_OIII	Distance (") in DEC between the KC with the [OIII] component and the ON
KCRA_OIII_ERR	KCRA_OIII uncertainty
KCDEC_OIII_ERR	KCDEC_OIII uncertainty
PX_V/VHA/VOIII	Number of unmasked pixels in the stellar, Hα and [OIII] velocity maps
FLAG	If FLAG == 'REVISAR', the ON is far from the center of the image.

Table 1 – Datamodel of the tables generated for kinematic analysis of the full MaNGA sample of galaxies and the sub-sample of the first six thousand galaxies observed through mid-2018 included in the MaNGA AGN catalog.

G. CONCLUSIONS

In this work, we have found that it is possible to use the same techniques used in García-Lorenzo et al. (2015) to analyse galaxy velocity maps from the MaNGA survey using the stellar and ionized gas (Hα and [OIII]) kinematics by generating their velocity gradient maps and estimating the location of their kinematic center and their gradient peak structure. While the automatisation of the latter is harder and we haven't found a way to implement it in this work, we have been able to generate tables for the full MaNGA sample of galaxies with information on their kinematic center estimation and other relevant galactic properties.

We have found that, while in García-Lorenzo et al. (2015) they identified a direct relationship between galaxies with significant offsets between the optical nucleus and their kinematic center and their interacting status, in all the samples studied in this work there is a non-negligible percentage of isolated galaxies that present significant offsets. There are therefore other factors other than the galaxy interactions that can cause these offsets.

After taking a closer look to the isolated galaxy sub-sample, we have found that there seems to be a tendency towards lower masses for isolated galaxies with significant offsets. We can assume that this might be because lower mass galaxies might not have reached the dynamical equilibrium needed for them to move as pure rotating disks.

Moreover, it is important to remember that any departure of the galaxy from moving as a pure rotating can manifest as a shift in the gradient peak position and structure. Therefore, a deeper analysis is needed in order to complete the research done in this work.

Finally, we leave the tables and important codes used during the development of this work at the disposition of the research group, in order to facilitate the continuation of the analysis through any of the points listed in the future work section (`https://github.com/acasasbuenas/mangagradients`).

References

Argudo-Fernández, M., Verley, S., Bergond, G., Puertas, S. D., Carmona, E. R., Sabater, J., Lorenzo, M. F., Espada, D., Sulentic, J., Ruiz, J., et al. (2015). Catalogues of isolated galaxies, isolated pairs, and isolated triplets in the local Universe. *Astronomy & Astrophysics*, 578.

Blanton, M. R., Kazin, E., Muna, D., Weaver, B. A., and Price-Whelan, A. (2011). Improved background subtraction for the sloan digital sky survey images. *The Astronomical Journal*, 142(1):31.

Bundy, K., Bershady, M. A., Law, D. R., Yan, R., Drory, N., MacDonald, N., Wake, D. A., Cherinka, B., Sánchez-Gallego, J. R., Weijmans, A.-M., et al. (2014). Overview of the SDSS-IV MaNGA survey: mapping nearby galaxies at Apache Point Observatory. *The Astrophysical Journal*, 798(1).

Cherinka, B., Andrews, B. H., Sánchez-Gallego, J., Brownstein, J., Argudo-Fernández, M., Blanton, M., Bundy, K., Jones, A., Masters, K., Law, D. R., et al. (2019). Marvin: A tool kit for streamlined access and visualization of the SDSS-IV MaNGA data set. *The Astronomical Journal*, 158(2):74.

Comerford, J. M., Negus, J., Müller-Sánchez, F., Eracleous, M., Wylezalek, D., Storchi-Bergmann, T., Greene, J. E., Barrows, R. S., Nevin, R., Roy, N., et al. (2020). A catalog of 406 AGNs in mAnga: A connection between radio-mode AGNs and star formation quenching. *The Astrophysical Journal*, 901(2).

Domínguez Sánchez, H., Margalef, B., Bernardi, M., and Huertas-Company, M. (2022). SDSS-IV DR17: final release of MaNGA PyMorph photometric and deep-learning morphological catalogues. *Monthly Notices of the Royal Astronomical Society*, 509(3).

Ellison, S. L., Patton, D. R., Mendel, J. T., and Scudder, J. M. (2011). Galaxy pairs in the Sloan Digital Sky Survey – IV. Interactions trigger active galactic nuclei. *Monthly Notices of the Royal Astronomical Society*, 418(3):2043–2053.

Feng, S., Shen, S.-Y., Yuan, F.-T., Dai, Y. S., and Masters, K. L. (2022). The Velocity Map Asymmetry of Ionized Gas in MaNGA. I. The Catalog and General Properties. *The Astrophysical Journal Supplement Series*, 262(1):6.

García-Lorenzo, B., Márquez, I., Barrera-Ballesteros, J., Masegosa, J., Husemann, B., Falcón-Barroso, J., Lyubenova, M., Sánchez, S., Walcher, J., Mast, D., et al. (2015). Ionized gas kinematics of galaxies in the CALIFA survey-I. Velocity fields, kinematic parameters of the dominant component, and presence of kinematically distinct gaseous systems. *Astronomy & Astrophysics*, 573:A59.

Kauffmann, G., Heckman, T. M., Tremonti, C., Brinchmann, J., Charlot, S., White, S. D., Ridgway, S. E., Brinkmann, J., Fukugita, M., Hall, P. B., et al. (2003). The host galaxies of active galactic nuclei. *Monthly Notices of the Royal Astronomical Society*, 346(4):1055–1077.

Sánchez, S., Kennicutt, R., De Paz, A. G., Van de Ven, G., Vílchez, J., Wisotzki, L., Walcher, C., Mast, D., Aguerri, J., Albiol-Pérez, S., et al. (2012). CALIFA, the Calar Alto Legacy Integral Field Area survey-I. Survey presentation. *Astronomy & Astrophysics*, 538:A8.

Sánchez, S., Pérez, E., Sánchez-Blázquez, P., González, J., Rosález-Ortega, F., Cano-Díaz, M., López-Cobá, C., Marino, R., Gil de Paz, A., Mollá, M., et al. (2016). Pipe3D, a pipeline to analyze integral field spectroscopy data: I. New fitting philosophy of FIT3D. *Revista mexicana de astronomía y astrofísica*, 52(1):21–54.

Verdes-Montenegro, L., Sulentic, J., Lisenfeld, U., Leon, S., Espada, D., Garcia, E., Sabater, J., and Verley, S. (2005). The AMIGA project-I. Optical characterization of the CIG catalog. *Astronomy & Astrophysics*, 436(2):443–455.

Westfall, K. B., Cappellari, M., Bershady, M. A., Bundy, K., Belfiore, F., Ji, X., Law, D. R., Schaefer, A., Shetty, S., Tremonti, C. A., et al. (2019). The data analysis pipeline for the SDSS-IV MaNGA IFU galaxy survey: overview. *The Astronomical Journal*, 158(6):231.